




Ultrafast structural relaxation dynamics of laser-excited graphene: *Ab initio* molecular dynamics simulations including electron-phonon interactions

Sergej Krylow ^{1,*}, Felipe Valencia Hernandez,² Bernd Bauerhenne ¹ and Martin E. Garcia ^{1,†}

¹Theoretical Physics and Center for Interdisciplinary Nanostructure Science and Technology (CINSAT),

Universität Kassel, 34132 Kassel, Germany

²National University of Colombia, 404 Building, Ciudad Universitaria, 111321 Bogota, Colombia



(Received 12 July 2019; revised manuscript received 16 January 2020; accepted 6 May 2020; published 26 May 2020)

The time evolution of the lattice structure in graphene after ultrashort laser excitation results in a complex dynamics of electrons and ions. In particular, a femtosecond laser pulse heats up the electrons, which then couple strongly to particular optical phonon modes, called SCOPs (strongly coupled optical phonons), located around the Γ and K (K') points of the Brillouin zone. In this paper, a fully *ab initio* description of the ultrafast structural response of graphene to femtosecond laser excitation is presented. Our atomistic simulations show that upon intense ultrafast laser excitation, a biexponential decay of the Bragg peaks takes place, in agreement with experiments. The calculated time-dependent phonon energies show that SCOPs equilibrate considerably faster with phonons having frequencies above 10 THz than with lower frequency phonon modes.

DOI: [10.1103/PhysRevB.101.205428](https://doi.org/10.1103/PhysRevB.101.205428)

I. INTRODUCTION

Graphene and its allotropes are intensively studied due to their unique properties, like high heat conductivity [1], extraordinary electrical conductivity [2–4], and extreme structural strength [5,6]. Based on the above characteristics, numerous applications in electronics [7–9], heat management [10], photonics [11,12], and as a composite material [6,12] are possible. Especially for electronics, it is crucial to understand the electron-electron, electron-phonon, and phonon-phonon scattering processes after the excitation of the system by time-dependent electric fields. In particular, it is widely accepted that the strong coupling between the electronic system and specific optical phonon modes at the Γ and K (K') points, called strongly coupled optical phonons (SCOPs), are of major importance for the high-field electronic transport [13]. All three types of scattering processes are relevant for the equilibration of graphitic materials after ultrafast laser excitation because the equilibration of the system proceeds in three stages [14–21]. First, the electronic system acquires a defined temperature, then SCOPs are generated and, finally, the SCOPs equilibrate with the other phonons, leading to the thermalization of the complete system. The relevant timescales and interactions, which are believed to take place in graphene upon laser excitation, are shown schematically in Fig 1. Pump-probe optical experiments, commonly used in the analysis of the ultrafast dynamical response, yield indirect information about the contribution of the scattering processes [14,15,19,22,23]. Direct information can rather be obtained by ultrafast electron diffuse scattering

measurements [24] and interpreted using density-functional theory calculations [25,26].

Here, we report on the first *ab initio* molecular dynamics (MD) simulations of the ultrafast lattice motions in graphene after excitation with an intense ultrafast laser pulse. Beginning from a thermalized electronic system, we model the coupling of the electrons to the lattice using a modified two-temperature model molecular dynamics (TTM-MD) approach, which is based on *ab initio* determination of the laser-excited potential energy surface and of the electron-phonon coupling. With this approach, we obtain results for the time evolution of the (100) and (110) families of Bragg peaks that are consistent with time-resolved diffraction experiments. Furthermore, we analyze ultrafast relaxation processes in deeper detail by calculating the time evolution of the energies and occupations of the different phonon modes allowed in our simulation supercell. Our approach yields the presence of SCOPs, which are rapidly excited by the hot electrons. The SCOPs themselves decay by exciting phonon modes with frequencies above 10 THz, whereas equilibration with lower frequency modes happens on a considerably larger timescale.

II. METHODS

A. Modeling of the electron-phonon coupling

Electron-hole pairs are created in solids after excitation with a femtosecond laser pulse. The electron-hole pairs thermalize on a very short timescale, during which the ions remain cold. The resulting hot electrons transfer energy to the lattice through electron-phonon interactions. This exchange results in a decrease of the electronic temperature, and ultimately leads to the equilibration of the electrons and the phonons. In our paper, we use and adapt the TTM-MD developed in

* krylow@physik.uni-kassel.de

† Corresponding author: m.garcia@uni-kassel.de

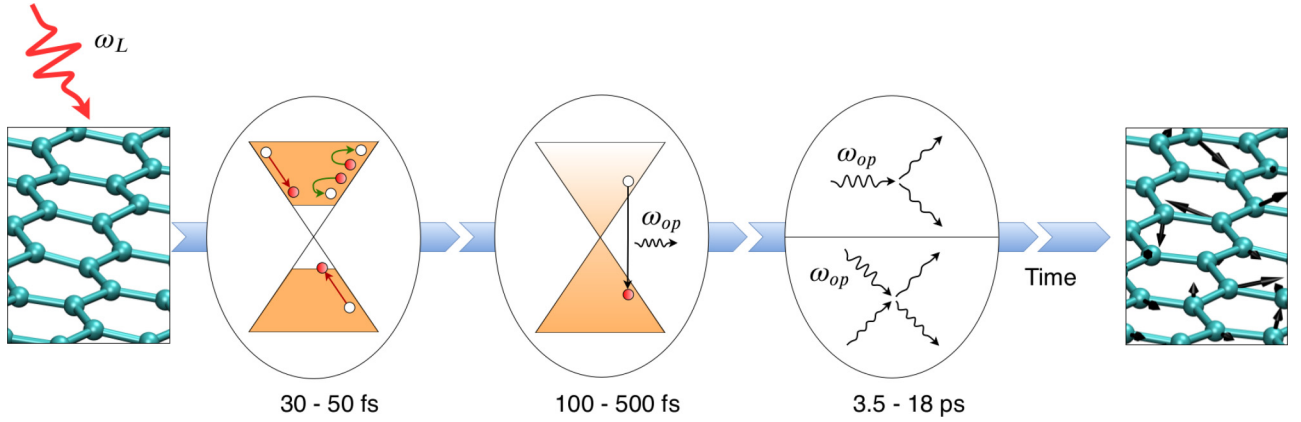


FIG. 1. Schematic time evolution of the current view on the relaxation of graphene after laser excitation, including the relevant timescales. After the laser excitation (left), the electronic system equilibrates first due to Auger processes (green arrows) and impact scattering (red arrows) within about 30–50 fs. Shortly afterwards, the recombination of electrons and holes generates SCOPs (middle) with frequencies ω_{op} on a timescale of 100–500 fs. Then, the SCOPs decay within 3.5–18 ps into other phonon modes via third- and fourth-order interactions, yielding a heated lattice in nonequilibrium (right).

Ref. [27], which describes the energy exchange between hot electrons, characterized by a temperature $T_e(t)$, and the ions, described through Newton’s equation of motion. The model is based on the assumption that a laser pulse mainly interacts with the electrons and thus creates a nonequilibrium between electrons and ions. We consider a supercell containing N atoms. The energy changes inside the electronic system are described in terms of a differential equation for the electronic temperature, which reads

$$NC_{V,at}(T_e) \frac{dT_e}{dt} = \frac{dU_{laser}(t)}{dt} - G_{ep}(T_e, T_I) \times (T_e - T_I), \quad (1)$$

where $C_{V,at}(T_e)$ is the electronic heat capacity at constant volume per atom, $T_e(t)$ the electronic temperature, and t the time. The first term on the right-hand side corresponds to the laser source term, where $U_{laser}(t)$ is the absorbed laser energy integrated up to time t . The second term describes the coupling between electrons and phonons by the electron-phonon coupling constant G_{ep} , which depends on the temperature of the electrons T_e and ions T_I .

The general TTM-MD method [27] couples the rate Eq. (1) for the electronic temperature to Newton’s equations of motion of the ions via a friction/antifricition term which accounts for the electron-phonon interactions. The motion of the ions can thus be written in compact form as

$$\frac{d\mathbf{p}}{dt} - \mathbf{f} - \xi \mathbf{p} = 0, \quad (2)$$

where $\mathbf{p} = (p_{1x}, p_{1y}, p_{1z}, \dots, p_{Nx}, p_{Ny}, p_{Nz})$ is a $3N$ -dimensional vector containing the momenta of all atoms and $\mathbf{f} = (\vec{\nabla}_1 \Phi, \dots, \vec{\nabla}_N \Phi)$ contains the forces acting on all atoms calculated as gradients of the interatomic potential Φ . The term proportional to \mathbf{p} reflects the electron-phonon interactions and represents a damping ($\xi < 0$) when energy of the ions is transferred to electrons, and an antidamping ($\xi > 0$) when the ions absorb energy from the electrons. The damping/antidamping factor ξ is proportional to the

temperature difference ($T_e - T_I$) and to the electron-phonon coupling constant G_{ep} [27].

In this paper, we use a generalized version of the TTM-MD and introduce a series of improvements. First, we use an extended version of Eq. (1) and allow a distinction between groups of phonons coupling differently to electrons. This idea was previously used for other materials [28,29], and yields a more general differential equation for the electronic temperature, which can be written as

$$NC_{V,at}(T_e) \frac{dT_e}{dt} = \frac{dU_{laser}}{dt} - \sum_{\nu} n_{\nu} G_{ep}^{(\nu)}(T_e, T_I^{(\nu)}) \cdot (T_e - T_I^{(\nu)}). \quad (3)$$

Here, each group ν contains n_{ν} phonons, has a particular electron-phonon coupling constant G_{ep}^{ν} , and a temperature $T_I^{(\nu)}$. Note that G_{ep}^{ν} is the electron-phonon coupling constant per phonon group. The classification in phonon groups makes sense for graphene because it is known from experiments that the SCOPs couple more strongly to electrons than to other types of phonons.

To have a consistent picture, we now project the equations of motion for the ions [Eq. (2)] into the phonon degrees of freedom. For this, we write the momenta and forces in terms of their projections onto the phonon eigenvectors \mathbf{e}_i , which yields

$$\mathbf{p} = \sum_i \frac{(\mathbf{e}_i \mathbf{p})}{\sqrt{m}} \sqrt{m} \mathbf{e}_i = \sum_i P_i \sqrt{m} \mathbf{e}_i \quad (4)$$

and

$$\mathbf{f} = \sum_i \frac{(\mathbf{e}_i \mathbf{f})}{\sqrt{m}} \sqrt{m} \mathbf{e}_i = \sum_i F_i \sqrt{m} \mathbf{e}_i. \quad (5)$$

Here, m is the mass of a carbon atom, P_i the projection of the momentum, and F_i the projection of the force onto the phonon mode $i = 1, \dots, 3N$. The phonon eigenvectors are calculated by diagonalizing the dynamical matrix. Throughout this paper, we assume that the phonon eigenvectors do not change in

time. From Eqs. (4) and (5), the equation of motion Eq. (2) becomes

$$\sum_i \left[\frac{dP_i}{dt} - F_i - \xi^{(\nu)} P_i \right] \sqrt{m} e_i = 0 \quad (6)$$

or, equivalently,

$$\frac{dP_i}{dt} - F_i - \xi^{(\nu)} P_i = 0, \quad i = 1, \dots, 3N, \quad (7)$$

since the eigenvectors e_i are linearly independent. The superscript ν denotes the group of phonons which have a similar coupling to the electrons and to which mode i belongs to. $\xi^{(\nu)}$ is given by [27]

$$\xi^{(\nu)} = \frac{n_\nu G_{ep}^{(\nu)} (T_e - T_I^{(\nu)})}{2E_{\text{kin}}^{(\nu)}}. \quad (8)$$

Equation (7) couples the electronic subsystem to phonon i , which is in the ν th group of phonon modes. Notice that the damping/antidamping force term $\xi^{(\nu)} P_i$ decelerates/accelerates the phonon i in its current direction of movement depending on whether the electronic temperature T_e is smaller/larger than the temperature $T_I^{(\nu)}$ of the phonons in group ν . The kinetic energy of each phonon group $E_{\text{kin}}^{(\nu)}$ reads

$$E_{\text{kin}}^{(\nu)} = \frac{\sum_{j \in \{\nu\}} (P_j^* P_j)}{2}. \quad (9)$$

For the calculation of the lattice temperature $T_I^{(\nu)}$ in Eqs. (3) and (7), we use the equipartition theorem, which states that

$$E_{\text{kin}}^{(\nu)} = \frac{n^{(\nu)} k_B T_I^{(\nu)}}{2}, \quad (10)$$

where k_B is the Boltzmann constant.

The main improvements of the present paper are (i) the MD simulations are *ab initio*; this means that the forces on the ions are obtained as the gradients of the laser-excited potential energy surface calculated via density-functional theory using a generalized Born-Oppenheimer approximation (see below) instead of using an analytical interatomic potential, and (ii) the electron-phonon coupling constants $G_{ep}^{(\nu)}$ are also calculated from first principles. In this way, we provide a full *ab initio* description of the ultrafast nonequilibrium lattice dynamics of graphene after femtosecond laser excitation.

B. Electron-phonon coupling calculation details

To evaluate the electron-phonon coupling constants $G_{ep}^{(\nu)}(T_e, T_I^{(\nu)})$ for Eqs. (3) and (8), we treat graphene as a metal and use the formalism developed in Refs. [30,31], which are based on the Allen formalism and the Eliashberg function [32]. In this framework, the electron-phonon coupling G_{ep} can be written as

$$G_{ep} = -\frac{2\pi}{g(\epsilon_F)(T_e - T_I)} \times \int_0^\infty \left[d\omega (\hbar\omega)^2 \alpha^2 F(\omega) (n(\omega, T_e) - n(\omega, T_I)) \right] \times \int_{-\infty}^\infty d\epsilon g^2(\epsilon) \frac{\partial f(\epsilon, T_e)}{\partial \epsilon}. \quad (11)$$

Here, $f(\epsilon, T)$ and $n(\omega, T)$ are the Fermi-Dirac and Bose-Einstein occupation factors at the electron energy ϵ and phonon frequency ω . The parameter $g(\epsilon)$ is the electronic density of states, ϵ_f the Fermi energy, and $\alpha^2 F(\omega)$ the Eliashberg spectral function, given by

$$\alpha^2 F(\omega) = \frac{1}{2\pi g(\epsilon_f)} \sum_{q\nu} \frac{\gamma_{q\nu}}{\omega_{q\nu}} \delta(\omega - \omega_{q\nu}), \quad (12)$$

where

$$\gamma_{q\nu} = 2\pi \omega_{q\nu} \sum_{kmn} |M_{[k+q,n],[k,m]}^{q\nu}|^2 \times \delta(\epsilon_{k+q,m} - \epsilon_f) \delta(\epsilon_{k,n} - \epsilon_f). \quad (13)$$

The quantities $|M_{[k+q,n],[k,m]}^{q\nu}|$ correspond to the electron-phonon coupling matrix elements and $\omega_{q\nu}$ the frequency of phonon ν at q in reciprocal space. The evaluation of the summations over delta functions in Eqs. (12) and (13) requires the use of a Gaussian smearing function with a broadening parameter σ_d .

For the calculations of the electron-phonon coupling and the Eliashberg function, we use the QUANTUM ESPRESSO package [33]. We employ the local density approximation and a Hartwigsen-Goedecker-Hutter pseudopotential with a 120 Ry cutoff for the kinetic energy of the plane waves. For the ground state and vibrational mode calculations, we use a Monkhorst-Pack grid of 42×42 k points, and a Fermi-Dirac smearing of the electronic states, $\sigma_0 = 0.003$ Ry (~ 473 K). With these calculation parameters, we obtain an accurate description of the phonon frequencies. The phonon linewidths were further interpolated to a finer mesh of 252×252 k points [34]. Because of the ultrafast laser excitation, the electronic states and electron-phonon interactions are considerably broadened. To account for this, we use three broadening factors σ_d with values of 0.025 (3947 K), 0.035 (5526 K), and 0.05 Ry (7894 K), respectively. Note, that a simpler two-temperature model was previously used to model the time evolution of the electrons and the SCOPs of graphene in Ref. [17].

C. *Ab initio* MD simulation details

For simulating graphene, we use our in-house Code for Highly Excited Valence Electron Systems (CHIVES), which is an electronic-temperature-dependent density-functional theory MD code [35]. It uses the local density approximation, [36] atom-centered Gaussian basis sets [37], relativistic pseudopotentials [38,39], and periodic boundary conditions. For graphene, we consider an orthorhombic simulation supercell with $N = 180$ carbon atoms, a time step of 0.5 fs and a $2 \times 2 \times 1$ k-space grid. The equation of motion is solved using the Velocity-Verlet algorithm, for which the forces f are obtained as gradients from the laser-excited potential energy surface, which is given by the Mermin functional [40], obtained from finite-temperature density-functional theory. The laser excitation is modeled by increasing the electronic temperature, where the change of the electronic temperature due to the laser pulse is given by $\frac{dU_{\text{laser}}(t)}{dt}$ in Eq. (3). In this paper, we consider two different pulse forms. In the first case, we use an ideal delta pulse. This results in an instantaneous

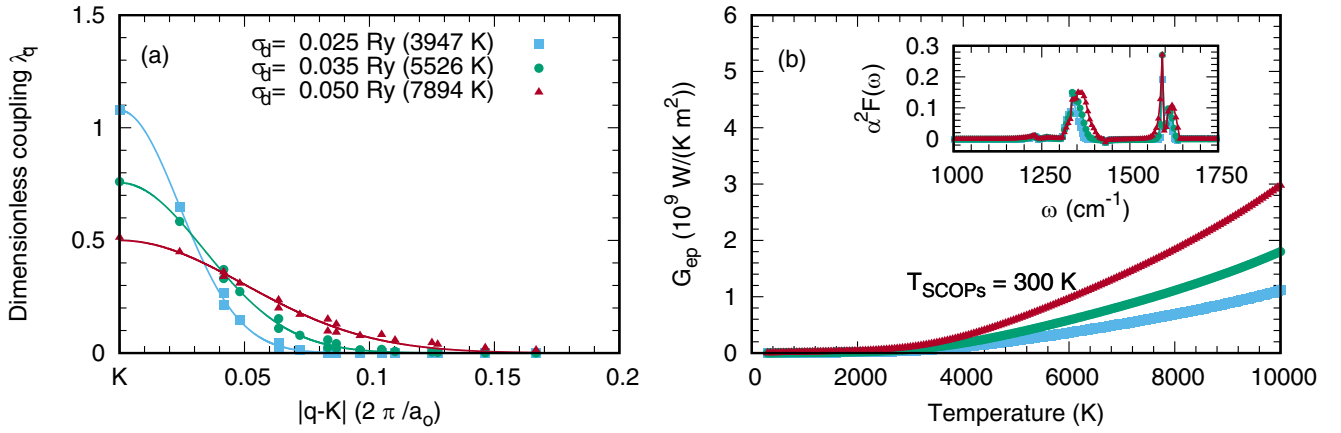


FIG. 2. (a) Adimensional e-ph coupling parameter calculated for optical modes near the K point, using different Gaussian broadening parameters σ_d . (b) Coupling coefficient G_{ep} as a function of the electronic temperature, calculated using different Gaussian broadening parameters σ_d . The inset shows the Eliashberg function for the used broadening parameters.

increase of the electronic temperature at 0 ps to 8000 K. In the second case, we assume a Gaussian laser pulse centered at 0 fs with a FWHM of 40 fs, so $U_{\text{laser}}(t)$ becomes an error function. We approximate the absorbed fluence of both pulses to $56 \frac{\mu\text{J}}{\text{cm}^2}$. Our assumption that the electrons are always equilibrated is reasonable because the electronic system reaches a well-defined electronic temperature within about 30–50 fs after irradiation in graphene and graphite [14–18]. The analyzed time period in this paper is considerably larger than this one. To sample the phase space in our simulation, we have generated 20 MD runs using the method described in Ref. [21]. All presented results are averaged over these 20 runs for the results from the *ab initio* MD simulation. The ionic temperature T_I entering in Eq. (3) is calculated “on the fly” from the computed velocities using the equipartition theorem [Eq. (10)]. In each MD time step, we average $T_I^{(v)}$ over 20 parallel running simulations. This smooths the time evolution of $T_I^{(v)}$, which would otherwise fluctuate considerably because of the limited size of our supercell. We also use CHIVES to *ab initio* determine heat capacity of the electrons $C_{V,at}$ entering in Eq. (3). For this purpose, we calculate the change of the total energy of the system with respect to the electronic temperature. The ions are fixed at their equilibrium positions during the calculation of $C_{V,at}$.

III. RESULTS AND DISCUSSION

A. Calculation of the electron-phonon coupling

Equation (3) describes the coupling between groups of phonons to the electronic subsystem. To identify the groups of phonons, which strongly couple to electrons in graphene, we analyze both the dimensionless coupling parameter λ_q given by

$$\lambda_q = \frac{\gamma_{qv}}{\pi \hbar g(\epsilon_F) \omega_{qv}^2}, \quad (14)$$

which is based on the calculations of Eq. (13) in Sec. II B, and the Eliashberg function. The dimensionless coupling parameter λ_q helps to locate the regions in q space where such phonons are present, without giving energy resolution. λ_q is shown in Fig. 2(a) in the vicinity of the K point for

the assumed broadening parameters σ_d . It is evident that the electron-phonon coupling is only nonzero near the K point. For increasing electronic temperatures, the coupling decreases directly at the K point, but modes in the q points in the near vicinity become more important. This can be explained by the considerable broadening of the Fermi distribution due to the ultrafast laser excitation. The same behavior can be seen at the K' and Γ points. Thus, only phonons around these q points contribute to the electron-phonon coupling and the contribution of the other phonon modes is negligible. This means that the quantity λ_q can clearly identify the q points at which the SCOPs are located. A Gaussian with a variance σ can be fitted to the dimensionless coupling parameter in Fig. 2(a). The obtained variances are about $0.024 \cdot 2\pi/a_0$, $0.033 \cdot 2\pi/a_0$, and $0.05 \cdot 2\pi/a_0$ for the broadening parameters σ_d of 3947 K, 5526 K, and 7894 K, respectively. The variance can be used to define a radius r_{SCOP} , within which the q points with the SCOPs are distributed. In our simulation, we use a radius r_{SCOP} of $0.1 \cdot 2\pi/a_0$, which is about two times the variance at a broadening parameter σ_d of 7894 K. Ideally, the radius r_{SCOP} should be smaller but in that case only the K , K' , and Γ points would contribute to the electron-phonon coupling and the dynamics of the simulation would be quite different from experimental observations. This discrepancy is caused by the limited supercell size for which the distances between q points in reciprocal space are larger than σ . Increasing the supercell size would solve this problem but would make the simulation computationally unfeasible. Note that not all phonons at the q points, at which λ_q is large, contribute to the electron-phonon coupling. For a frequency resolution, we need to analyze the Eliashberg function, which is plotted in the inset of Fig. 2(b). The Eliashberg function shows that only phonons with frequencies near 1350 (40.5 THz) and 1600 cm^{-1} (48 THz) contribute to the electron-phonon coupling. Near the K and K' points, the three highest phonon branches have phonon frequencies near 1350 cm^{-1} (40.5 THz), so SCOPs are the phonons with those frequencies. At the Γ point, the two highest phonon branches have frequencies near 1600 cm^{-1} (48 THz) and these phonon modes are also SCOPs. Directly at the K and K' points, the SCOPs can be identified by comparing the eigenvectors obtained from the electron-phonon

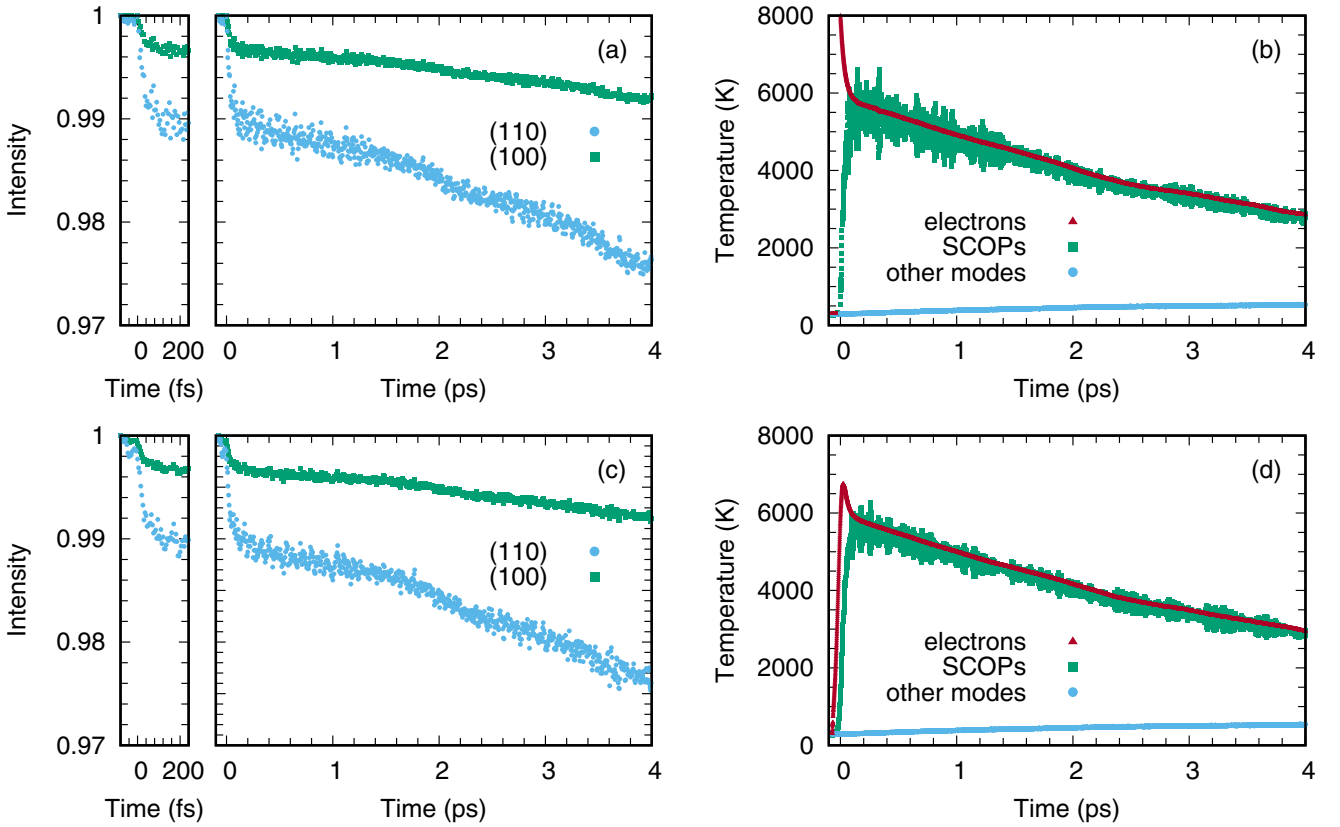


FIG. 3. (a), (c) Time evolution of the normalized intensities of the (100) and (110) Bragg peaks in graphene for the delta pulse (a) and the Gaussian pulse (c). (b), (d) Time evolution of the temperature of the SCOPs, the other phonon modes, and the electrons for the delta pulse (b) and the Gaussian pulse (d).

coupling calculations with the ones from the *ab initio* MD simulations. This not possible for the other \mathbf{q} points. In total, we obtain 20 SCOPs for our supercell of 180 atoms. We have shown above that only a subset of phonon modes contribute to the electron-phonon coupling in graphene. Therefore, we can simplify Eq. (3) to

$$NC_{V,at}(T_e) \frac{dT_e}{dt} = \frac{dU_{\text{laser}}(t)}{dt} - n_{\text{SCOP}} G_{ep}^{(\text{SCOP})}(T_e, T_l^{(\text{SCOP})}) \times (T_e - T_l^{(\text{SCOP})}), \quad (15)$$

where the sum over ν vanishes because only SCOPs couple to the electronic subsystem. Here, we made the simplification that all SCOPs couple equally to the electronic subsystem to make the interpretation of results easier. This assumption is reasonable since the average Eliashberg function in Fig. 2(b) is similar for the low (40.5 THz) and high (48 THz) frequency SCOPs.

Figure 2(b) shows the electron-phonon coupling parameter G_{ep} in dependence of the electronic temperature for the used broadening parameters σ_d and a lattice temperature of 300 K for the SCOPs. The electron-phonon coupling constants increase monotonically for increasing electronic temperatures. The dependence of the electron-phonon coupling parameter G_{ep} on the temperature of the SCOPs is considerably smaller than on the electronic temperature. The difference between the coupling constant at the same electronic temperature but at different SCOP temperatures in the range of 50 to 6000 K

does not exceed 9.6×10^7 , 1.5×10^8 , and $2.5 \times 10^8 \frac{\text{W}}{\text{Km}^2}$ for the broadenings of 3947 K, 5526 K, and 7894 K, respectively. Note, that the SCOPs have a small heat capacity because they are only a small subset of all phonons. Since electrons only couple to the SCOPs, the temperature of the SCOPs can reach high values, eventually higher than the melting threshold of graphene. For our *ab initio* MD simulations, we use the coupling constants obtained with a broadening of $\sigma_d = 5526$ K.

B. Time evolution of the Bragg peaks after laser excitation.

Using the calculated electron-phonon coupling constants, we have performed *ab initio* MD simulations on graphene. Details of the simulations are given in Sec. II C. We first analyze the time evolution of the Bragg peaks $I(\{\mathbf{q}\}, t)$ after ultrafast laser excitation, which are calculated by

$$I(\{\mathbf{q}\}, t) = \frac{|\sum_j \sum_{i=1}^N \exp(i\mathbf{q}_j \times \mathbf{r}_i(t))|^2}{|\sum_j \sum_{i=1}^N \exp(i\mathbf{q}_j \times \mathbf{r}_i(0))|^2}. \quad (16)$$

The first sum is over all peaks of the same family with reciprocal lattice vectors \mathbf{q}_j . The second sum is over all atoms N located at positions \mathbf{r}_i . Figures 3(a) and 3(c) show the obtained results for the (100) and (110) families of peaks of graphene using the delta pulse and the Gaussian laser pulse, respectively. A fast initial decay of the Bragg peaks and a slower decay afterwards can be seen. The slower decay shows

an increase of the decay rate in time, which is not visible in experiments. We attribute this to the time-dependent change of the decay channels for the SCOPs. This can be expected because the electron-phonon coupling changes the electronic temperature, which in turn modifies the potential energy surface and with that the frequencies of the phonon modes. Thus, due to energy conservation, decay channels might close or open up in time. This will also occur in real systems. However, real systems have infinite phonon modes, so the opening or closing of decay channels leads to smooth changes. In our simulations, such changes will occur discretely. A considerable increase of the number of atoms would solve the problem, but an extension of the computational cell is not possible because modern density-functional theory codes are limited to about 1000 atoms. Note that heat conduction becomes important after about 4–5 ps, which will also influence the dynamics of the system [41].

A biexponential function of the form

$$I_{\text{fit}}(t) = I_0 + A(1 - \exp(t/\tau_1)) + B(1 - \exp(t/\tau_2)) \quad (17)$$

cannot fit our data because of the modification of the decay channels described above. Nevertheless, we see that the fast initial decay is faster than 100 fs and the long decay is in the order of several ps. Thus, the obtained decay is consistent with the experimentally observed ones for graphite and graphene, which usually range from 100 to 500 fs for the fast decay and from 3.5 ps to 18 ps for the long decay [14–18,22,42]. Other theoretical works also suggested short decay times below 100 fs [42,43].

C. Change of the temperatures in time

The time-dependent temperatures of the electrons, SCOPs, and of the remaining phonon modes are shown in Fig. 3(b) for the delta pulse and Fig. 3(d) for the Gaussian pulse. Two timescales govern the temperature evolution for the electrons and SCOPs. For the delta pulse, the electronic temperature drops within the first 100 fs after laser excitation and then decays more slowly. For the Gaussian pulse, on the other hand, a fast increase of the electronic temperature within the first 100 fs can be seen. After that, the electronic temperature starts to decay due to the coupling to the SCOPs. For both considered pulses, a fast initial increase of the temperature of the SCOPs is visible. After its first increase, the temperature of the SCOPs starts to decrease due to phonon-phonon interactions. During this decrease, the temperature of electrons and SCOPs converge to each other due to the strong electron-phonon coupling. The temperature of the other phonon modes increases slowly and nearly linearly. Note that the heat capacity of the other modes is much higher than the heat capacity of the SCOPs. Thus, the decrease of the temperature of the SCOPs is stronger than the increase of the temperature of the other phonon modes. Similar to the Bragg peak analysis, the dynamics are independent of the used laser pulse form for long times. Therefore, we will use the results from the delta pulse excitation for the further analysis.

For small supercells, as considered in this paper, the details of the simulation will depend on the size of the supercell.

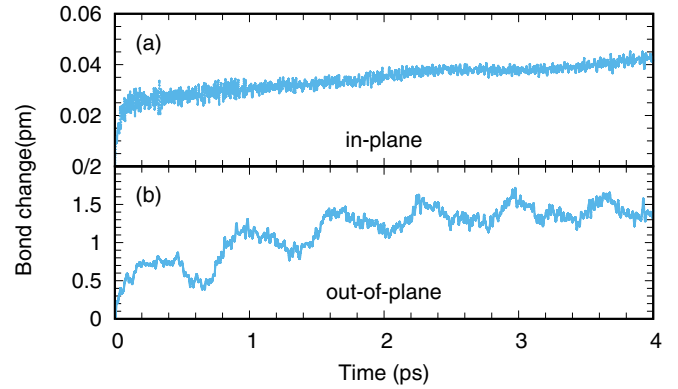


FIG. 4. Time evolution of the average change of the bond-length [Eq. (18)] projected onto the in-plane (a) and out-of-plane (b) motions.

This can be seen in the Supplemental Material in Ref. [44], where calculations of the time evolution of the Bragg peaks and temperatures for a supercell with 96 atoms are shown. The details are the same except that we have 40 instead of 20 runs over which we average. Note that the radius r_{SCOP} for choosing the q points, in which the SCOPs are in, were chosen as described before. For the supercell of 96 atoms, 20 SCOPs are also obtained. Although the Bragg peaks have the same dynamics, the time evolution of the temperatures are different. This can be explained as follows. The absorbed fluence per atom is equal for both systems but the total absorbed energy is larger for the greater supercell. However, the total absorbed energy is distributed between the same amount of SCOPs, so the temperature of the SCOPs and electrons is higher if the supercell is larger. In general, the number of SCOPs will depend on the size of the supercell. For the supercell sizes used here, the number of SCOPs is limited due to the large distance between q points as described before. Nevertheless, the temperature in thermal equilibrium will be equal for both supercell sizes. Although the time evolution of the temperatures depends on the used supercell in our calculations, our simulations clearly demonstrate that the fast decay is caused by the SCOPs and the further decay by the other phonon modes. Thus, we further analyze the dynamics obtained for the supercell of 180 atoms.

D. Time evolution of the nearest neighbor distance

Next, we analyze the time evolution of the average bond length d_N between carbon atoms after ultrafast laser excitation. For every atom i on position r_i a set of nearest neighbors $\{nn\}_i$ can be defined, so d_N can be written as

$$d_N(t) = \frac{\sum_{i=1}^N \sum_{j \in \{nn\}_i} (|r_i(t) - r_j(t)|)}{2N_{\text{bonds}}}. \quad (18)$$

The first sum is over all atoms, the second one over the set $\{nn\}_i$, and N_{bonds} is the total number of bonds between the carbon atoms. The distance $|r_i - r_j|$ can be further split into an in-plane and an out-of-plane part. Figures 4(a) and 4(b) show $\Delta d_N(t) = d_N(t) - d_N(t=0)$ for the in-plane and out-of-plane dynamics. For the in-plane dynamics of $\Delta d_N(t)$, a fast initial increase and a much slower increase after about

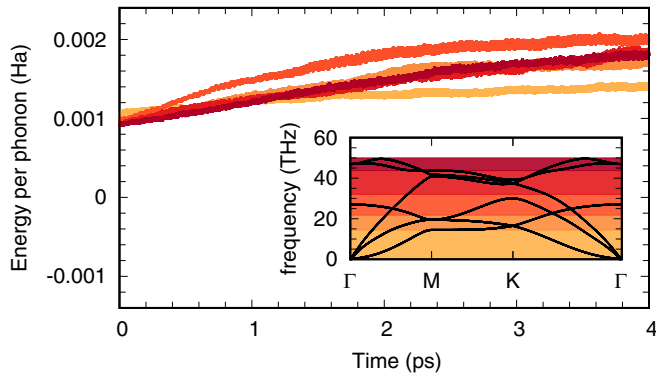


FIG. 5. Average energy per phonon mode for phonons in ascending frequency ranges. In each frequency range, indicated by the coloring of the phonon dispersion in the inset, we have included 104 phonon modes. The width corresponds to the errors. Note that we excluded the SCOPs from the analysis.

100 fs can be seen. The out-of-plane dynamics shows an oscillatory behavior and a general monotonic increase of $\Delta d_N(t)$ during the analyzed time period. The out-of-plane oscillation is induced by the fast increase of the electronic temperature. This oscillation is not related to the generation of SCOPs because they also appear without considering electron-phonon coupling. Furthermore, the out-of-plane part of $\Delta d_N(t)$ exhibits a greater amplitude than the in-plane part. This can be explained by the restoring forces, which are considerably larger for the in-plane motion of the atoms than for the out-of-plane motion.

E. Decay channels in graphene

To analyze the dynamics of graphene in more detail and to infer the pathways during the equilibration process, we have calculated the time evolution of the energies per phonon mode after laser excitation. For the calculation of the energies per phonon mode, we use the formalism described in Ref. [45]. Since the equilibrium positions in graphene are not constant, as can be seen in Figs. 4(a) and 4(b), we calculate the energy of a phonon ν as $2E_{\text{kin}}^{\nu}$. Note that the kinetic energy of a single phonon mode is averaged over the used 20 runs, which have different starting positions and velocities. Thus, on average, the kinetic and potential energy of a single phonon mode fulfills the equipartition theorem. After the calculation of the single phonon energies, we average over sets of phonon modes. For the used sets, we group the 104 phonon modes exhibiting the lowest frequencies together, then the next 104 phonon modes, and so on. In this way, we have generated five sets of phonon modes. Note that we have excluded the SCOPs from this analysis. The time evolution of the averaged energy per phonon mode and per set is shown in Fig. 5. In the inset, the phonon dispersion at the ground state and the frequency ranges of the five sets are shown. The time evolution of the average energies shows different slopes. In particular, the energy of midfrequency phonon modes increases the most and the energy of low-frequency phonon modes increases the least. All other sets of phonon modes have essentially the same slope for the time-dependent energy per phonon mode. From this analysis, we can conclude that the initial drop of the intensity

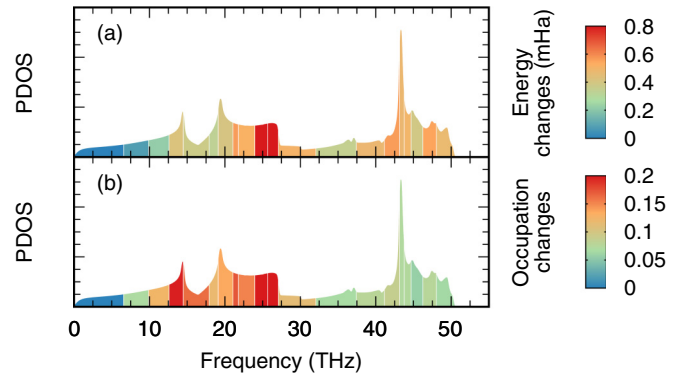


FIG. 6. Time-averaged changes of the energy (a) and phonon occupation number (b) with respect to their initial values for phonon sets containing 26 phonons.

in Figs. 3(a) and 3(c) is due to the generation of SCOPs rather than a fast decay into other phonon modes as suggested in Ref. [46]. From this coarse-grained analysis, it is not possible to see the dominant decay paths. Therefore, we increase the number of sets so each set contains 26 phonons. Furthermore, we take a time average over the whole simulation time of 4 ps. The average change of the energy with respect to the energy at $t = 0$ ps is shown in Fig. 6(a). The frequency ranges of the sets and the average change of the energy are shown as the colored areas incorporated into the phonon density of states. Additional information can be gained by calculating the average change of the phonon occupation numbers during the simulation, which is shown in Fig. 6(b). Note that the maximum error for the energy is about 0.06 mHa. The errors for the phonon occupation numbers are about 50% for the two lowest sets and about 10–30% for the other ones. From the analysis shown in Figs. 6(a) and 6(b), it is evident that many different phonons couple to the SCOPs. In particular, mainly phonons in the range from 10 to about 32 THz couple to the SCOPs. This range of phonons is consistent with the results for the third-order coupling of Ref. [25]. In particular, it was found that the SCOPs near the Γ point couple to phonons in the range from 18 to 30 THz and the SCOPs near the K (K') point couple to phonons in the region from 12 to 27 THz. However, it was also claimed that for the SCOPs near the K and K' points, the dominant third-order scattering involves phonons near 3 and 37 THz. In this regions, we obtain no indications for a dominant coupling of this kind. There are several possible reasons for this discrepancy. First, we analyze laser-excited graphene in our simulations. Thus, the potential energy surfaces, and with that the coupling strengths between the phonon modes might be different. Second, scattering events after the scattering from the SCOPs to the other phonon modes will influence the decay of the SCOPs. Third, our supercell might not contain the phonons to which the SCOPs near the K and K' points couple dominantly. Additionally, to the decay channels discussed above, we can also see that phonons between 40 and 50 THz gain a considerable amount of energy. This decay path was not reported in Ref. [25]. Since all third-order scattering processes were analyzed in Ref. [25], we have to assume that the increase of the energy in this frequency region is due to fourth-order scattering processes.

IV. CONCLUSIONS

In conclusion, we have used *ab initio* MD simulations and a modified TTM-MD model to simulate the time evolution of laser-excited graphene. For that, we have calculated the electron-phonon coupling constants for various electronic and ionic temperatures. Our results show that not only the SCOPs at the Γ point and K (K') point are important for the electron-phonon coupling in the laser-excited case but also the phonons in the near vicinity of these points. This is due to the smearing of the Fermi function caused by the high electronic temperature in the laser-excited case. Based on the obtained electron-phonon coupling constants, we have performed *ab initio* MD simulations. With our simulations, we are able to simulate the time evolution of the (100) and (110) families of Bragg peaks after laser excitation. In particular, we obtain a biexponential decay for the analyzed Bragg peaks. The short decay time is below 100 fs and the long decay is in the order of several ps, which is consistent with ultrafast

pump-probe experiments on graphene and graphite. Furthermore, we can show that the SCOPs are mainly decaying into phonons with phonon frequencies between 10 to 32 THz and to a smaller extent into phonons in the 40 to 50 THz range. The former frequency region fits well to the dominant third-order scattering events reported in Ref. [25]. We account the other frequency range to fourth-order scattering events.

ACKNOWLEDGMENTS

We gratefully acknowledge the support from Deutsche Forschungsgemeinschaft through the projects GA 465/15-2 and GA 465/18-1. B. Bauerhenne gratefully acknowledges the financial support from the Otto-Braun-Fonds and the “Abschlussstipendium der Universität Kassel”. Calculations for this research were conducted on the Lichtenberg high performance computer of the TU Darmstadt. The visualization of the used supercell in Fig. 1 was done with VMD (<http://www.ks.uiuc.edu/Research/vmd/>) [47].

-
- [1] A. A. Balandin, S. Ghosh, W. Bao, I. Calizo, D. Teweldebrhan, F. Miao, and C. N. Lau, *Nano Lett.* **8**, 902 (2008).
 - [2] K. S. Novoselov, A. K. Geim, S. V. Morozov, D. Jiang, Y. Zhang, S. V. Dubonos, I. V. Grigorieva, and A. A. Firsov, *Science* **306**, 666 (2004).
 - [3] K. S. Novoselov, A. K. Geim, S. V. Morozov, D. Jiang, M. I. Katsnelson, I. V. Grigorieva, S. V. Dubonos, and A. A. Firsov, *Nature* **438**, 197 (2005).
 - [4] C. Berger, Z. Song, X. Li, X. Wu, N. Brown, C. Naud, D. Mayou, T. Li, J. Hass, A. N. Marchenkov, E. H. Conrad, P. N. First, and W. A. de Heer, *Science* **312**, 1191 (2006).
 - [5] C. Lee, X. Wei, J. W. Kysar, and J. Hone, *Science* **321**, 385 (2008).
 - [6] R. J. Young, I. A. Kinloch, L. Gong, and K. S. Novoselov, *Compos. Sci. Technol.* **72**, 1459 (2012).
 - [7] M. J. Allen, V. C. Tung, and R. B. Kaner, *Chem. Rev.* **110**, 132 (2010).
 - [8] M. Y. Han, B. Özyilmaz, Y. Zhang, and P. Kim, *Phys. Rev. Lett.* **98**, 206805 (2007).
 - [9] M. C. Lemme, T. J. Echtermeyer, M. Baus, and H. Kurz, *IEEE Electron Device Lett.* **28**, 282 (2007).
 - [10] S. Ghosh, I. Calizo, D. Teweldebrhan, E. P. Pokatilov, D. L. Nika, A. A. Balandin, W. Bao, F. Miao, and C. N. Lau, *Appl. Phys. Lett.* **92**, 151911 (2008).
 - [11] F. Bonaccorso, Z. Sun, T. Hasan, and A. C. Ferrari, *Nat. Photon.* **4**, 611 (2010).
 - [12] K. S. Novoselov, V. I. Fal’ko, L. Colombo, P. R. Gellert, M. G. Schwab, and K. Kim, *Nature* **490**, 192 (2012).
 - [13] T. Kampfrath, L. Perfetti, F. Schapper, C. Frischkorn, and M. Wolf, *Phys. Rev. Lett.* **95**, 187403 (2005).
 - [14] M. Breusing, S. Kuehn, T. Winzer, E. Malić, F. Milde, N. Severin, J. P. Rabe, C. Ropers, A. Knorr, and T. Elsaesser, *Phys. Rev. B* **83**, 153410 (2011).
 - [15] M. Breusing, C. Ropers, and T. Elsaesser, *Phys. Rev. Lett.* **102**, 086809 (2009).
 - [16] J. C. Johannsen, S. Ulstrup, F. Cilento, A. Crepaldi, M. Zacchigna, C. Cacho, I. C. Edmond Turcu, E. Springate, F. Fromm, C. Raidel, T. Seyller, F. Parmigiani, M. Grioni, and P. Hofmann, *Phys. Rev. Lett.* **111**, 027403 (2013).
 - [17] C. H. Lui, K. F. Mak, J. Shan, and T. F. Heinz, *Phys. Rev. Lett.* **105**, 127404 (2010).
 - [18] H. Wang, J. H. Strait, P. A. George, S. Shivaraman, V. B. Shields, M. Chandrashekar, J. Hwang, F. Rana, M. G. Spencer, C. S. Ruiz-Vargas, and J. Park, *Appl. Phys. Lett.* **96**, 081917 (2010).
 - [19] R. P. Chatelain, V. R. Morrison, B. L. M. Klarenaar, and B. J. Siwick, *Phys. Rev. Lett.* **113**, 235502 (2014).
 - [20] Y. Ishida, T. Togashi, K. Yamamoto, M. Tanaka, T. Taniuchi, T. Kiss, M. Nakajima, T. Suemoto, and S. Shin, *Sci. Rep.* **1**, 64 (2011).
 - [21] P. J. Hale, S. M. Hornett, J. Moger, D. W. Horsell, and E. Hendry, *Phys. Rev. B* **83**, 121404 (2011).
 - [22] S. Schäfer, W. Liang, and A. H. Zewail, *New J. Phys.* **13**, 063030 (2011).
 - [23] M. Scheuch, T. Kampfrath, K. Wolf, C. Volkman, L. Frischkorn, and L. Perfetti, *Appl. Phys. Lett.* **99**, 211908 (2011).
 - [24] M. J. Stern, L. P. René de Cotret, M. R. Otto, R. P. Chatelain, J.-P. Boisvert, M. Sutton, and B. J. Siwick, *Phys. Rev. B* **97**, 165416 (2018).
 - [25] N. Bonini, M. Lazzeri, N. Marzari, and F. Mauri, *Phys. Rev. Lett.* **99**, 176802 (2007).
 - [26] S. Butscher, F. Milde, M. Hirtschulz, E. Malic, and A. Knorr, *Appl. Phys. Lett.* **91**, 203103 (2007).
 - [27] D. S. Ivanov and L. V. Zhigilei, *Phys. Rev. B* **68**, 064114 (2003).
 - [28] Z. Lu, A. Vallabhaneni, B. Cao, and X. Ruan, *Phys. Rev. B* **98**, 134309 (2018).
 - [29] L. Waldecker, T. Vasileiadis, R. Bertoni, R. Ernstorfer, T. Zier, F. H. Valencia, M. E. Garcia, and E. S. Zijlstra, *Phys. Rev. B* **95**, 054302 (2017).
 - [30] X. Y. Wang, D. M. Riffe, Y.-S. Lee, and M. C. Downer, *Phys. Rev. B* **50**, 8016 (1994).
 - [31] L. Waldecker, R. Bertoni, R. Ernstorfer, and J. Vorberger, *Phys. Rev. X* **6**, 021003 (2016).
 - [32] P. B. Allen, *Phys. Rev. Lett.* **59**, 1460 (1987).

- [33] P. Giannozzi, O. Andreussi, T. Brumme, O. Bunau, M. B. Nardelli, M. Calandra, R. Car, C. Cavazzoni, D. Ceresoli, M. Cococcioni, N. Colonna, I. Carnimeo, A. D. Corso, S. de Gironcoli, P. Delugas, R. A. DiStasio, A. Ferretti, A. Floris, G. Fratesi, G. Fugallo, R. Gebauer, U. Gerstmann, F. Giustino, T. Gorni, J. Jia, M. Kawamura, H.-Y. Ko, A. Kokalj, E. Küçükbenli, M. Lazzeri, M. Marsili, N. Marzari, F. Mauri, N. L. Nguyen, H.-V. Nguyen, A. O. de-la Roza, L. Paulatto, S. Poncé, D. Rocca, R. Sabatini, B. Santra, M. Schlipf, A. P. Seitsonen, A. Smogunov, I. Timrov, T. Thonhauser, P. Umari, N. Vast, X. Wu, and S. Baroni, *J. Phys.: Condens. Matter* **29**, 465901 (2017).
- [34] M. Wierzbowska, S. de Gironcoli, and P. Giannozzi, [arXiv:cond-mat/0504077](https://arxiv.org/abs/cond-mat/0504077).
- [35] E. S. Zijlstra, T. Zier, B. Bauerhenne, S. Krylow, P. M. Geiger, and M. E. Garcia, *Appl. Phys. A* **114**, 1 (2014).
- [36] J. P. Perdew and Y. Wang, *Phys. Rev. B* **45**, 13244 (1992).
- [37] E. S. Zijlstra, N. Huntmann, A. Kalitsov, M. E. Garcia, and U. von Barth, *Modell. Simul. Mater. Sci. Eng.* **17**, 015009 (2009).
- [38] S. Goedecker, M. Teter, and J. Hutter, *Phys. Rev. B* **54**, 1703 (1996).
- [39] C. Hartwigsen, S. Goedecker, and J. Hutter, *Phys. Rev. B* **58**, 3641 (1998).
- [40] N. D. Mermin, *Phys. Rev.* **137**, A1441 (1965).
- [41] G. Barbarino, G. Fugallo, C. Melis, F. Mauri, and L. Colombo, *Phys. Rev. B* **94**, 245437 (2016).
- [42] M. Harb, H. Enquist, A. Jurgilaitis, F. T. Tuyakova, A. N. Obraztsov, and J. Larsson, *Phys. Rev. B* **93**, 104104 (2016).
- [43] W.-K. Tse, E. H. Hwang, and S. Das Sarma, *Appl. Phys. Lett.* **93**, 023128 (2008).
- [44] See Supplemental Material at <http://link.aps.org/supplemental/10.1103/PhysRevB.101.205428> for the time evolution of the Bragg peaks and temperatures for a supercell with 96 atoms.
- [45] S. Krylow, E. S. Zijlstra, F. C. Kabeer, T. Zier, B. Bauerhenne, and M. E. Garcia, *Phys. Rev. Mater.* **1**, 073601 (2017).
- [46] F. Carbone, P. Baum, P. Rudolf, and A. H. Zewail, *Phys. Rev. Lett.* **100**, 035501 (2008).
- [47] W. Humphrey, A. Dalke, and K. Schulten, *J. Mol. Graphics* **14**, 33 (1996).